Since January 2020 Elsevier has created a COVID-19 resource centre with free information in English and Mandarin on the novel coronavirus COVID-19. The COVID-19 resource centre is hosted on Elsevier Connect, the company's public news and information website.

Journal of Photochemistry & Photobiology, A: Chemistry 419 (2021) 113453

Contents lists available at ScienceDirect

Journal of Photochemistry & Photobiology, A: Chemistry

journal homepage: www.elsevier.com/locate/jphotochem

Synthesis of modified beta bismuth oxide by titanium oxide and highly efficient solar photocatalytic properties on hydroxychloroquine degradation and pathways

Fatemeh Kargar [a], Akram Bemani [a,*], Mohammad Hossein Sayadi [a,b], Najmeh Ahmadpour [b]

[a] Department of Environmental Sciences and Engineering, Faculty of Agriculture and Natural Resources, Ardakan University, P.O. Box 184, Ardakan, Iran
[b] Department of Environmental Engineering, Faculty of Natural Resources and Environment, University of Birjand, Birjand, Iran

ARTICLE INFO

Keywords:
TiO_2/β-Bi_2O_3 nanocomposite
Solar light
Hydroxychloroquine
Photocatalytic mechanism

ABSTRACT

With the outbreak of coronavirus pandemic the use of Hydroxychloroquine increased. These compounds have harmful effects on the environment, such as generation of antibiotic-resistant bacteria; therefore, their degradation has been considered as one of the environmental challenges. The purpose of this research is to synthesize heterogeneous structure of TiO_2/β-Bi_2O_3 by hydrothermal method for solar degradation of Hydroxychloroquine. Then, the accurate characteristics of the synthesized samples were investigated by XRD, FESEM, TEM, XPS, UV–vis (DRS), and BET surface analyzer. Photocatalytic degradation of Hydroxychloroquine was studied under sunlight, and it was found that the visible light absorption of TiO_2 photocatalyst by mixing β-Bi_2O_3 nanoparticles was greatly increased and 91.89% of the degradation was obtained in 120 min of photocatalytic reaction. This improvement can be attributed to the increased specific surface area, efficient charge transfer, and reduced electron-hole recombination with the β-Bi_2O_3 compound. Kinetic studies also reacted to follow pseudo-first-order kinetics. Also, demonstrated high stability and recyclability for nanoparticles, so that after 6 cycles of using the catalyst in take, 70.59% degradation was performed. According to the results, the excellent photocatalytic degradation activity demonstrated by the TiO_2/β-Bi_2O_3, therefore, it is a potential candidate for the process of removing other organic contaminants from aqueous solutions.

1. Introduction

Water pollution is an important issue worldwide, and solving this problem requires the use of new principles to remove pollutants. The human need for water along with the limitation of water resources in terms of quantity and quality has led to the importance of purification and recovery of this vital substance [1]. Coronavirus (COVID-19) has become a global disaster and there is a strong search for effective drug treatment for it. In March 2020, hydroxychloroquine (HCQ) was recommended for the treatment of the new Covid-19 detected for the first time in China as of November 2019. In fact, in vitro studies have indicated a sure efficacy of HCQ against infection by COVID-19, and are now one of the most effective drugs in the treatment of COVID-19. Long-term use of hydroxychloroquine (HCQ) is a cornerstone in the treatment of this disease [2]. However, the entry of substances containing these pharmaceutical compounds into the environment occurs through the wastewater of the pharmaceutical industry, hospital effluents, and effluents from wastewater treatment plants, laboratory activities, and human and animal wastes [3]. The use of HCQ is causing unanticipated harm to the environment. When HCQ enters the environment, they will lead to pharmaceutical stability of pathogenic bacteria and cause extremely serious harm to aquatic organisms in the environment and human health. Due to the increasing spread of these drugs and the further entry of these compounds into the effluent and sewage, more than ever, the removal of drugs from water and wastewater sources needs attention. Pharmaceutical compounds are present in surface and groundwater, sewage and even drinking water in the μg/l and ng/l, and given that the health care and physical health of communities is an important and fundamental principle around the world, the degradation, and removal of these Materials are of particular importance [4]. Various technologies such as activated carbon adsorption, reverse osmosis, filtration, and biological methods are used to remove drugs.

* Corresponding author: Department of Environmental Sciences and Engineering, Faculty of Agriculture and Natural Resources, Ardakan University, P.O. Box 184, Ardakan, Iran
E-mail address: a.bemani@ardakan.ac.ir (A. Bemani).

https://doi.org/10.1016/j.jphotochem.2021.113453
Received 11 April 2021; Received in revised form 4 July 2021; Accepted 15 July 2021
Available online 21 July 2021

However, the results indicated that the use of the above methods causes the transfer of contaminants from one phase to another, their concentration, and finally the production of a new contaminant that requires further treatment [5]. Advanced oxidation (AOPs) is one of the most popular processes that is widely accepted today due to the low-cost and simplicity of the process to remove resistant organic pollutants [6]. Compared with other methods, the chemical oxidation technique chiefly attains the purpose of degrading contaminates via chemical reactions, which can completely degrade contaminants without generating pharmaceutical-resistant bacteria [7]. Advanced oxidation is a process based on the production of free radicals, especially hydroxyl, which successfully attacks contaminant molecules [8]. Hydroxyl radicals are produced in aqueous media using H_2O_2, UV/H_2O_2, UV/TiO_2, UV/ZnO, and other methods [9]. In recent decades, semiconductor photocatalysis is due to its environmental friendliness, cost-effectiveness, high efficiency, and excellent stability, which can convert abundant and clean solar energy into chemical energy, so this process is considered as a green technology for Water and wastewater treatment [10–11]. To date, numerous semiconductor photocatalysts such as TiO_2, ZnO, C_3N_4, WO_3, Ag_3PO_4, and $SrTiO_3$ have been investigated. However, TiO_2 is still considered a suitable photocatalyst due to its high chemical stability, low- cost, and environmentally friendly [12–13]. Due to its wide band gap energy and its low activity in visible light, the use of this nanoparticle is limited. Researchers have proposed many strategies to increase the photocatalytic properties of visible light by increasing the use of solar energy and improving the efficiency of charge separation, including doping, loading of metal particles and other semiconductors [14]. The fabrication of a heterogeneous photocatalyst is one of the inventive approaches to overcome these limitations, because doped semiconductor oxide can not only efficiently separate and transmit optical electrons-holes, but also extend the amplitude of the optical response by the narrow-band gap semiconductor [15]. Bismuth oxide (Bi_2O_3) is one of the heterogeneous components, with excellent attributes and narrow band gap (2 to 3.96 eV), high refractive index, good optical conductivity, and non-toxic properties, and high photocatalytic activity [16–17]. To these properties, Bi_2O_3 is used in applications such as gas sensing, fuel cell, and water purification [18].

Bi_2O_3 emerges five fuzzy forms: α- (monoclinic), β- (tetragonal), γ- (body-centered cubic), δ- (face-centered cubic) and ε- (triclinic) [19]. Among these forms, α-Bi_2O_3 is known as the constant phase at low temperature and δ-Bi_2O_3 is the stable phase at high temperature (729 °C), the other three forms of Bi_2O_3 have a metastable phase. β-Bi_2O_3, as a metastable phase, has recently been reported to have excellent photocatalytic activity relative to α-Bi_2O_3 [20]. β-Bi_2O_3 has the highest absorption in the visible light region because it has the lowest band gap (2.4 eV) and shows better photocatalytic performance under visible light radiation. Due to the β-Bi_2O_3 is an intrinsic p-type semiconductor with high mobility, it can therefore be used as an electron donor in photocatalytic processes. TiO_2 is an inherent n-type semiconductor, which can be used as an electron receptor and provides a pathway for the surface charge transfer. Based on this strategy in this study, a p-n heterogeneous photocatalyst is synthesized by binding β-Bi_2O_3 and TiO_2. Whereas HCQ is the most widely used drug for the treatment of COVID-19 [2]. So, the substances containing these pharmaceutical compounds into the environment occurs [3]. When HCQ enters the environment, they will lead to pharmaceutical stability of pathogenic bacteria and cause extremely serious harm to the environment and human health. The aim of this study was to clarify the mechanism of the degradation of HCQ in aqueous solution and improve its photodegradation efficiency. Therefore, TiO_2/β-Bi_2O_3 nanocomposite was synthesized by hydrothermal method and was used for the photodegradation of HCQ under solar light irradiation. Furthermore, the photodegradation mechanism of TiO_2/β-Bi_2O_3 for HCQ was explored.

2. Materials and methods

2.1. Materials

Sodium hydroxide (NaOH), hydrochloric acid (HCl), bismuth nitrate ($Bi(NO_3)_3{\cdot}5H_2O$) and nitric acid (HNO_3), citric acid ($C_6H_8O_7$), ethanol and titanium (IV) areopropoxides purchased from Merck, and was used without further purification. Hydroxychloroquine sulfate (HCQ) was prepared from Mofid Pharmaceutical Company. It should be noted that deionized water was used during photocatalytic synthesis and degradation experiments.

2.2. Preparation of β-Bi_2O_3 nanoparticles

Initially for the synthesis of β-Bi_2O_3, 00.9 g Bi $(NO_3)_3{\cdot}5H_2O$ was dissolved in 20 ml of HNO_3 at a concentration of 1 M. Then 0.3 g of citric acid was added to the solution and after stirring for 1 h, the NaOH solution was added dropwise until the pH of the solution reached 4. The resulting suspension was then placed at room temperature for 1 h. The suspension was then placed in an autoclave and then placed for 2 h at 180 °C. After the reaction, the resulting suspension placed at room temperature for 90 min to cool. The production precursor was centrifuged at 2500 rpm for 15 min and washed three times with deionized water and ethanol and then dried for 60 h at 60 °C. Finally, the precursor was calcined for 3 h at 350 °C and finally, β-Bi_2O_3 nanopowders were obtained [21].

2.3. Preparation of TiO_2/β-Bi_2O_3 nanocomposite

The preparation process of TiO_2/β-Bi_2O_3 nanocomposite was performed by hydrothermal method. For this purpose, in the first step, 10 ml of ethanol along with 20 ml of distilled water was added dropwise to 5 ml of titanium (IV) isopropoxide solution and stirred for 30 min. Then 5 ml of acetic acid was added to the resulting solution and finally 40% Bi_2O_3 was added to TiO_2. The resulting solution was placed in an autoclave at 160 °C for 24 h. Finally, after centrifugation at 2500 rpm for 20 min, the solution was washed several times with distilled water and placed in an oven at 80 °C for 8 h [22].

2.4. Investigation of physical properties of synthesized catalysts

The crystal structure of the TiO_2/β-Bi_2O_3 nanocomposite synthesized by the Rigaku MiniFlex 600 (XRD) radiation diffract meter was investigated using Cu Ka radiation as the X-ray source. Fourier transform infrared (FTIR) spectroscopy (Shimadzu, FTIR 1650 spectrophotometer, Japan) were also applied to determine the chemical features of the nanocomposite. X-ray photoelectron (XPS) spectroscopy was performed using AMICUS, Kratos Analytical (Shimadzu) spectroscopy to investigate the oxidation state and chemical environment of the elements in the sample. The morphology and morphology of the samples were studied by a field diffusion scanning electron microscope (FESEM; JEOLJSM-7600F) equipped with an energy scattering spectrometer (EDS). The detailed study of the structure and size of nanoparticles was performed using TEM analysis (Philips EM208S 100KV). Nanocomposite topography was determined using atomic force microscopy (AFM). Ultraviolet reflection spectrum (DRS) was recorded on UV–Vis spectroscopy (Shimadzu, UV-2550, Japan). The Brunauer-Emmett-Teller (BET) surface area and sample pore size distribution were studied in the N_2 adsorption analyzer (NOVA 2000e) the USA. Active free radicals were determined using electron paramagnetic resonance (EPR) in a Bruker ELEXSYS 500 spectrometer.

2.5. Photodegradation tests

A batch system was used to perform photodegradation experiments. The light used in the experiment was solar light and UV-A light. The

batch photocatalytic system in this study was exposed to direct sunlight with an intensity of 76–72 kW and UV-A light with a light density of 6 W. The parameters studied in this experiment include pH different [3,5,7], concentration of TiO_2/β-Bi_2O_3 nanocomposite as a catalyst (0.05, 0.1, 0.3, 0.4 g/L), hydroxychloroquine concentration (1, 10, 20, 40 mg/L), H_2O_2 concentration (1,2, 3, 4 mg.L^{-1}), temperature (10, 20, 40, and 60 °C) and irradiation time (5,10,15,20,30,45,60,90,120 min). (0.1 M) HCl and (0.1 M) NaOH were used to adjust the pH, and a magnetic stirrer at 70 rpm was used to blend the system. Photodegradation experiment in dark conditions and photolysis was also performed. It should be noted that before exposing the sample to sunlight, and UV-A light irritation, the solution was first stirred for 30 min in the dark to ensure an adsorption-adsorption balance between the TiO_2/β-Bi_2O_3 photocatalyst and the hydroxychloroquine drug. Over a period, 5 ml of the solution was extracted. After centrifugation at 2000 rpm for 15 min, the adsorption rate of hydroxychloroquine was measured by a spectrophotometer (UV-770 Brite) at 343 nm. Equation [1] was used to calculate the HCQ removal percentage [23]:

$$\text{Removal of HCQ}(\%) = \frac{C_0 - C_t}{C_0} \times 100$$

In the above relation, C_0 is the initial concentration of hydroxychloroquine sulfate, C_e is the final concentration of hydroxychloroquine sulfate.

3. Results and discussion

3.1. Structural characterizations of TiO_2/β-Bi_2O_3

3.1.1. XRD analysis

The crystalline properties of β-Bi_2O_3, TiO_2, and TiO_2/β-Bi_2O_3 nanoparticles were analyzed using the XRD method. As Fig. 1shows all diffraction peaks at 19.55,21.76, 25.63, 27.4, 32.15, 35.86, 37.35, 46.85, 48.46, 54.78 and 63.45°belong to the surface of (111), (020), (002), (121), (212), (113), (041), (104), (241), (225), and (161) crystals, which corresponds to the tetrahedral β-Bi_2O_3 (JCPDS No. 71–2274) [24]. The XRD peaks in TiO_2 show anatase peaks (JCPDS 00–021-1272) so that diffraction peaks are located at 25.63, 32.15, 35.85, 47.5, 53.85, 54.83, 57.15, 62.43°, which correspond to (101), (222), (311), (200), (422), (105), (511) and (204) anatase TiO_2 [10]. Peaks of β-Bi_2O_3, as well as TiO_2, were observed in the TiO_2/β-Bi_2O_3 nanocomposite.

3.1.2. Fourier transform infrared (FTIR)

Fig. 2 shows the absorption peaks of the β-Bi_2O_3, TiO_2 and TiO_2/β-Bi_2O_3 samples under the FTIR. The peak at 530 (cm^{-1}) corresponds to the symmetric tensile states of the Bi-O bond of Bi_2O_3 species [25]. In addition, a significant decrease is observed in the FTIR spectrum for the vibration mode at 1200–1700 (cm^{-1}), which is a characteristic of the NO_3 group [26].The absorption peak at 1086 (cm^{-1}) was attributed to group C-O. The absorption peak in the range of 1384 (cm^{-1}) can be observed to Ti-O vibration in TiO_2 [27]. Also, the peaks in 1618, 28 and 3252 (cm^{-1}) are attributed to O–H vibrations in the hydroxyl group that is absorbed by the water at the surface [28].

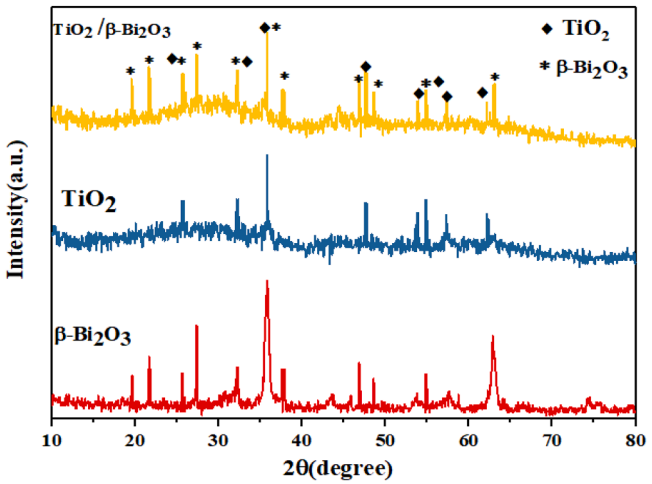

Fig. 1. XRD patterns for β-Bi_2O_3, TiO_2, and TiO_2/β-Bi_2O_3 nanocomposite.

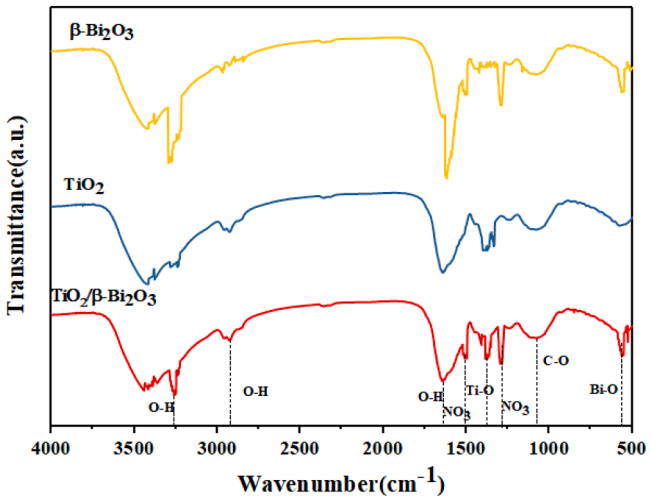

Fig. 2. FTIR spectra for β-Bi_2O_3, TiO_2, and TiO_2/β-Bi_2O_3 nanocomposite.

The presence of NO_3 in the FTIR spectrum is due to the thermal analysis of Bi $(NO_3)_3$ in the initial composition of bismuth oxide. Therefore, the absorption bands at 1200–1700 (cm^{-1}) show the presence of NO_3 groups [26]. Therefore, it can be stated that the hydroxyl and carboxyl, and NO_3 groups, respectively, are located in larger amounts on the surface of the particles of the samples, and according to the resulting nanoparticles it can cause better stability in the aquatic solution.

3.1.3. FESEM –EDX analysis for TiO_2, β-Bi_2O_3, and TiO_2/β-Bi_2O_3

The TiO_2, β-Bi_2O_3, and TiO_2/β-Bi_2O_3 nanoparticles are porous accumulates composed of smaller crystallizes. TiO_2 crystals have an average size of about 46 nm nanometers with a spherical shape (Fig. 3). β-Bi_2O_3 is formed as nanoparticles with an average size of about 37 nm (Fig. 3). FESEM images distribute the presence of spherical β-Bi_2O_3 nanoparticles evenly on the surface of TiO_2 particles. As can be seen, the particles using this preparation method are somewhat accumulated, which this accumulates may be attributed to the evaporation of organic matter adsorbed on the nanoparticle surface and structural changes as well as the lack of sonicates of the samples before imaging [5]. It can be concluded that, under the current path, bismuth metal nanoparticles are formed by hydrothermal reaction and after the calcination is completely transformed into TiO_2/β-Bi_2O_3 composite nanoparticles. In Fig. 3, the EDX spectra of the synthesized TiO_2/β-Bi_2O_3 compounds showed that Bi_2O_3 is well distributed in TiO_2 and there appears to be no separation of the two oxide phases. As can be seen, EDX analysis confirms the presence of β-Bi_2O_3 nanoparticles in TiO_2.

3.1.4. TEM analysis for TiO_2, β-Bi_2O_3, and TiO_2/β-Bi_2O_3

TEM images of composite nanoparticles (Fig. 4) showed that TiO_2 nanoparticles had a spherical shape with a diameter of approximately 67 nm. Fig. (4b), darker crystallites calculating about 42 nm in size are formed in the size of β-Bi_2O_3 crystals. Also, β-Bi_2O_3 nanoparticles were unstable under the electron rays of TEM and underwent structural arrangement. TEM images (4c) confirmed the presence of spherical β-Bi_2O_3 nanoparticles 16 nm in diameter uniformly on the surface of

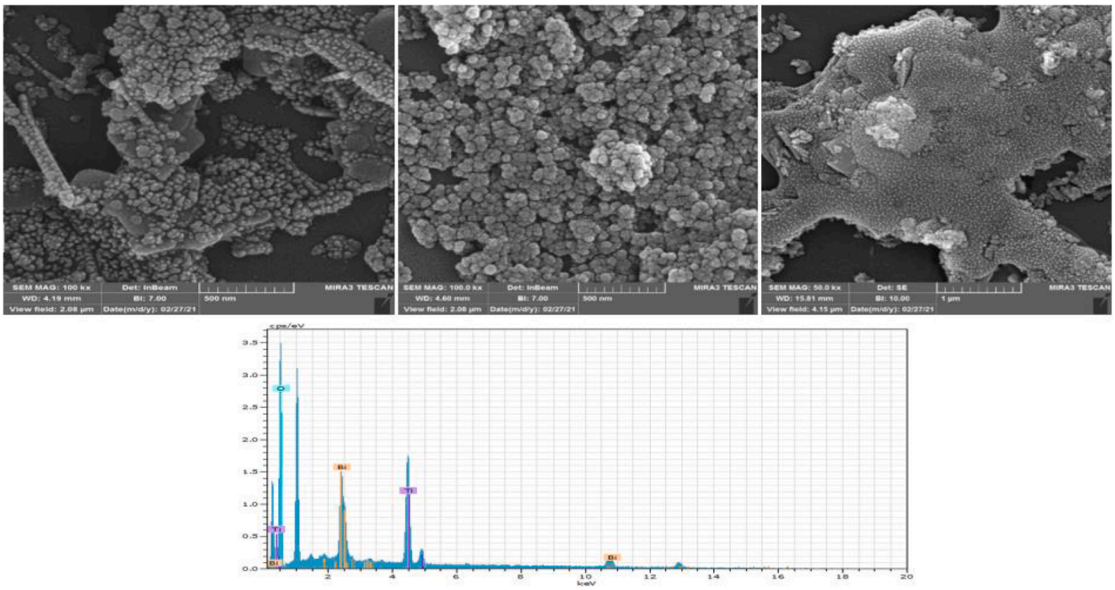

Fig. 3. FESEM images of TiO_2 nanoparticles, β-Bi_2O_3, TiO_2/β-Bi_2O_3 nanocomposite and EDX analysis of TiO_2/β-Bi_2O_3 nanocomposite.

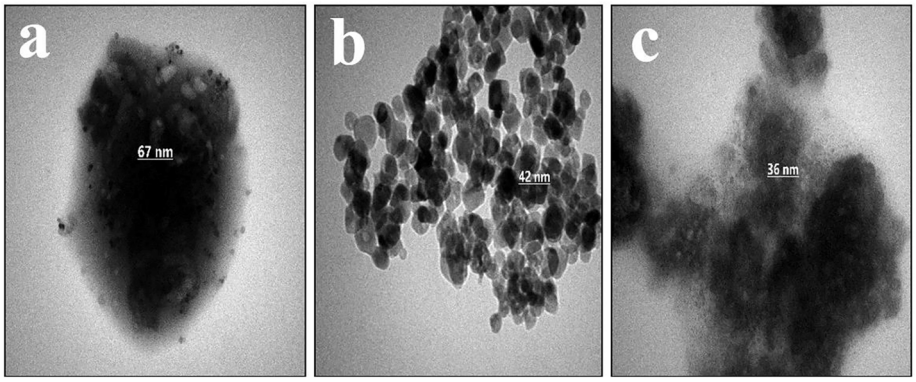

Fig. 4. TEM image of (a) TiO_2; (b) -β-Bi_2O_3; (c) TiO_2/β-Bi_2O_3 nanoparticles.

TiO_2 particles.

3.1.5. Atomic force microscopy (AFM) analysis for surface analysis of TiO_2/β-Bi_2O_3 layers

AFM analysis is possible to determine the roughness and predicted surface parameters of TiO_2/β-Bi_2O_3 layers. Fig. 5 shows an AFM micrograph of the surface of TiO_2/β-Bi_2O_3 layers. As can be seen, the surface of the TiO_2/β-Bi_2O_3 layers with Ra = 152 nm and Rq = 191 nm show a calculated surface area of 1.318 μm. This roughness is essential due to the dendritic growth of TiO_2/β-Bi_2O_3 layers to increase HCQ uptake and photocatalytic mineralization [29].

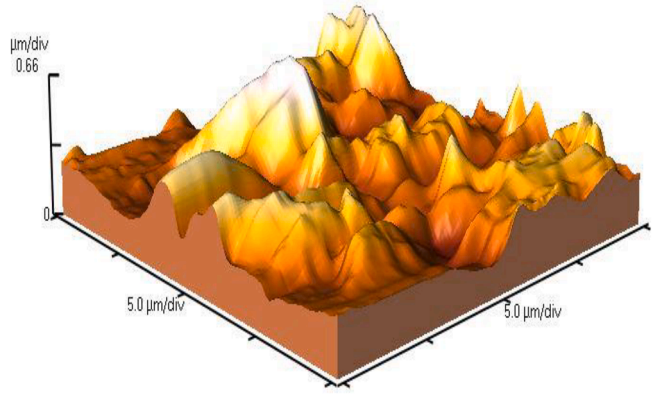

Fig. 5. AFM analysis of topographic micrographs of TiO_2/β-Bi_2O_3 surface layers.

3.1.6. XPS analysis for TiO_2/β-Bi_2O_3 nanoparticles

Existing compounds and chemical states of TiO_2/β-Bi_2O_3 composite nanoparticles were investigated using XPS analysis. As can be observed, the spectrum confirmed the presence of C, O, Ti, and Bi at the surface of β-Bi_2O_3/TiO_2. Fig. 6(a) (a) shows the XPS spectrum of TiO_2/β-Bi_2O_3. The binding energy spectrum of Ti 2p at 458.2 and 1/464 eV corresponds to Ti $2p_{3/2}$ and Ti $2p_{1/2}$ (Fig. 6b) [5]. Bi 4f symmetric peaks with axes of 164.1 and 159.5 eV are assigned to β-Bi_2O_3 (Fig. 6 c). Peaks at 539.5 and 530.4 eV were indicative of oxygen in β-Bi_2O_3 and TiO_2 (Fig. 6 d) [24].

3.1.7. Brunauer – Emmett – Teller (BET) level analysis for TiO_2/β-Bi_2O_3 nanocomposite

One of the effective factors in photocatalytic performance is BET sample specific regions, which are measured by nitrogen adsorption–desorption method. The samples synthesized in this study, according to the International Union of Pure and Applied Chemistry (IUPAC) classification, have mesoporous surface and show a type IV isotherm with a type H_3 residue. The BET level for the composite sample

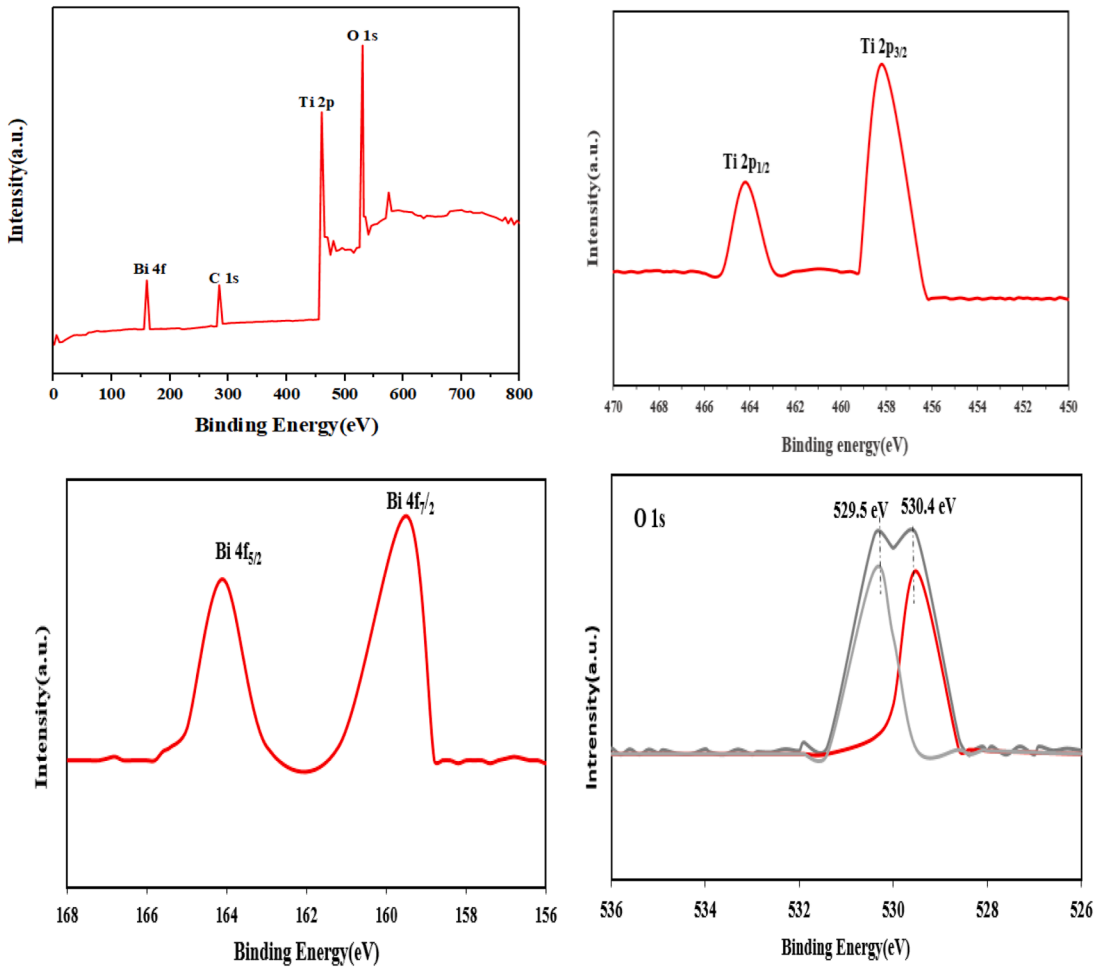

Fig. 6. XPS spectrum TiO_2/β-Bi_2O_3 nanocomposite. (a) Complete investigation of TiO_2/β-Bi_2O_3, (b) Ti, (c), Bi and (d). Oxygen.

was 156.7 m^2/g. It was also observed from the pore size distribution of BJH that the resulting sample has a narrow pore size distribution. The total pore volume was 0.394 cc/g. In this study, the average pore radius was 13.76 nm Fig 7.

3.1.8. *UV–vis spectrum analysis (DRS) for TiO_2, β-Bi_2O3 and TiO_2/β-Bi_2O_3 nanocomposite*

The UV–vis spectrum (DRS) was obtained from TiO_2, β-Bi_2O_3 and TiO_2/β-Bi_2O_3 samples and the results are shown in Fig. 8. Since TiO_2 showed high absorption in the UV region (200–400 nm) with a band gap

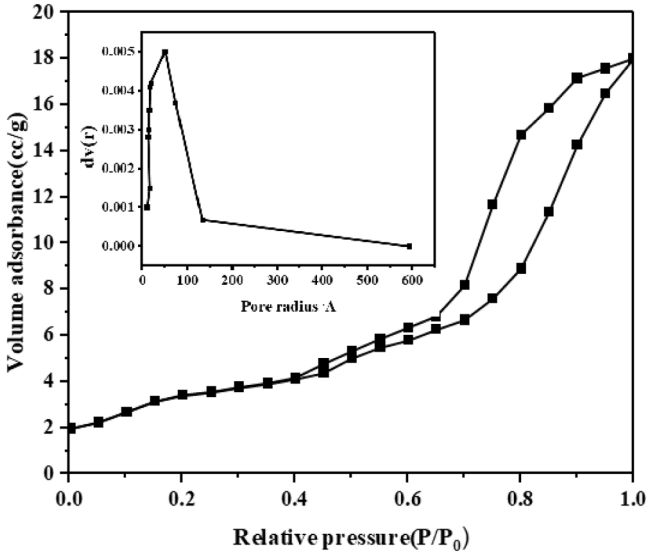

Fig. 7. Adsorption-desorption isotherm N_2 for TiO_2/β-Bi_2O_3. And BJH pore size distribution.

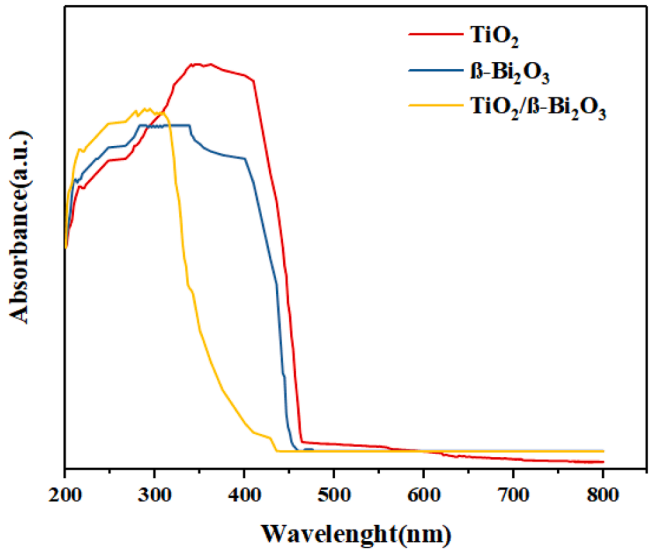

Fig. 8. The UV–vis spectrum (DRS) spectrum for the synthesized samples.

of 3.2 eV, which is typical for TiO_2 anatase. While β-Bi_2O_3 had more absorption in the visible light region, which showed a band gap energy of 2.46 eV [30]. While the UV spectrum of TiO_2/β-Bi_2O_3 composites is absorbed more light in the visible light region compared to TiO_2 and β-Bi_2O_3 [31]. Therefore, the highest visible light response among nanoparticles was related to TiO_2/β-Bi_2O_3 nanocomposite, which is attributed to the synergy effect between TiO_2 and β-Bi_2O_3. Therefore, this nanocomposite can be used in photocatalytic reactions due to better performance and more efficient use of light [12].

4. Analysis of electron paramagnetic resonance (EPR)

The recognition •OH in aqueous media was investigated by electron paramagnetic resonance (EPR) without adding pollutants. To investigate the role of active oxygen free radicals in the photocatalytic degradation of HCQ, trapping experiments with isopropyl alcohol (IPA), methyl alcohol (MA), and ammonium oxalate (AO) were added to trap the $\cdot O_2^-$, $^{\cdot}OH$, and h^+. As Fig. 9a shown, in the absence of sunlight irradiation, there was no definite peak relating to $DMPO^{-}$• OH, and in the ERP spectra, demonstrated that no ·OH will be produced in the absence of light irradiation of TiO_2/β-Bi_2O_3. After sunlight irradiation, the EPR spectrum with an intensity ratio of 1:2:2:1 signal was clearly observed, which related to the $DMPO^{-}$•OH [10]. Meanwhile, $^{\cdot}O_2^-$ was detected in methanol solution; the result is indicated in Fig. 9 (b). Without sunlight irradiation, there was no signal connected by DMPO-$^{\cdot}O_2^-$ appeared in the EPR spectrum. While, by irradiating sunlight to the TiO_2/β-Bi_2O_3 composite, a four-line special signal with an intensity ratio of 1: 1: 1: 1 is created in the EPR spectrum, which relates to the peak of DMPO-$^{\cdot}O_2^-$. These results showed that $^{\cdot}OH$ and $^{\cdot}O_2^-$ were produced in TiO_2/β-Bi_2O_3 in the photocatalytic process with sunlight irradiation.

4.1. Solar light–induced photodecomposition of HCQ

4.1.1. Effect of pH on photocatalytic degradation of HCQ

The pH of the reaction medium plays an important role in the oxidation process by the photocatalytic reaction. The pH value has a decisive effect on the oxidation potential of OH radicals due to the correlation between the oxidation potential and the pH value. Therefore, the role of pH in any photocatalytic reaction must be determined [19]. Therefore, in this study, the impact of pH on the degradation of HCQ using TiO_2/β-Bi_2O_3 catalyst in the pH range of 3–11 with a dose of 10 mg/L HCQ, 0.1 g/L catalyst and 0.1 $mg.L^{-1}$ H_2O_2 was examined at ambient temperature and in direct solar light irradiation. Fig. 10 shows the effect of pH on the degradation of hydroxychloroquine in the pH range from 3 to 11. The highest drug degradation was obtained by using

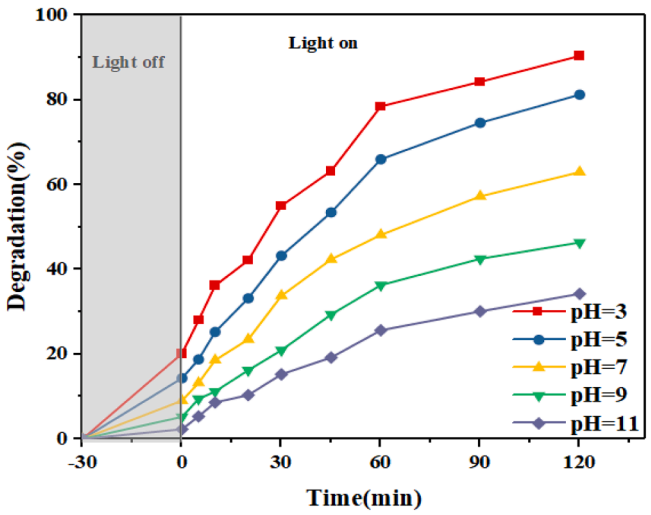

Fig. 10. Effect of pH on HCQ degradation.

a catalyst at pH 3 with 92.37%. It is assumed that the surface of β-Bi_2O_3/TiO_2 catalyst is positively charged in acidic solution while negatively charged in alkaline solution [32]. Also, the drug hydroxychloroquine is known as an organic substance that has a negative charge. Therefore, it is clear why the highest degradation is obtained at acidic pH compared to alkaline pH. The activity of the catalysts may be due to the presence of a strong electrostatic field between the surface of the positively charged catalyst and the negatively charged drug. This finding showed the important role of pH in the degradation of organic pollutants. Another reason for the increase in degradation in an acidic medium is the production of hydroxyl radicals, which were higher than in an alkaline medium, so these radicals can increase the oxidation potential. In addition, the oxidation potential due to the recombination of hydroxyl radicals in an acidic medium is lower than that of an alkaline [1]. At low pH, the adsorption of cationic organic molecules on the photocatalyst surface increases, because the photocatalyst surface has a positive charge, which leads to increased adsorption of cationic organic molecules. Therefore, the degradation efficiency increases at low pH .

4.1.2. Effect of temperature

The effect of temperature on the optical degradation of hydroxychloroquine molecules was investigated using TiO_2/β-Bi_2O_3 nanoparticles Fig 11. As the temperature increases, the photocatalytic degradation efficiency of HCQ molecules increases. Therefore,

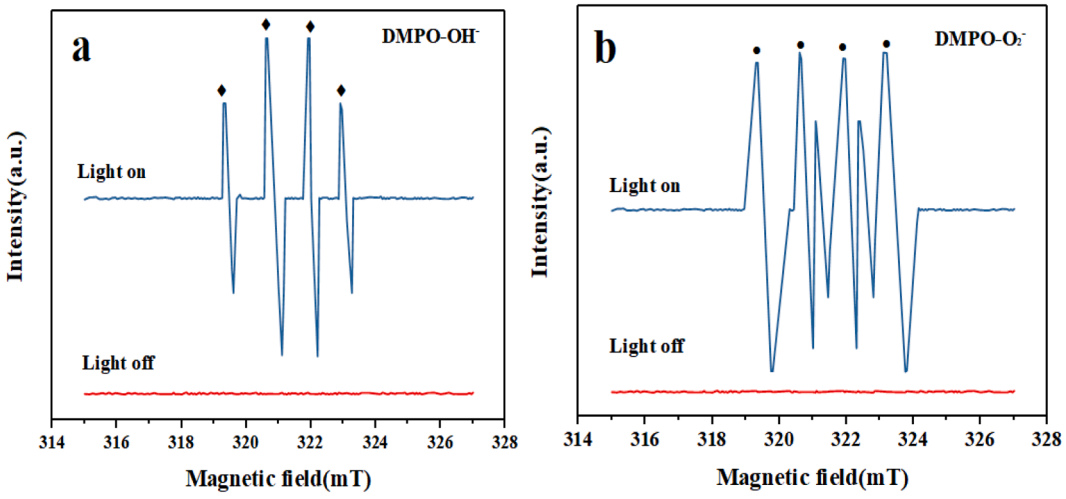

Fig. 9. EPR spectra of TiO_2/β-Bi_2O_3 a) DMPO-$^{\cdot}OH$ and b) DMPO-$^{\cdot}O_2^-$.

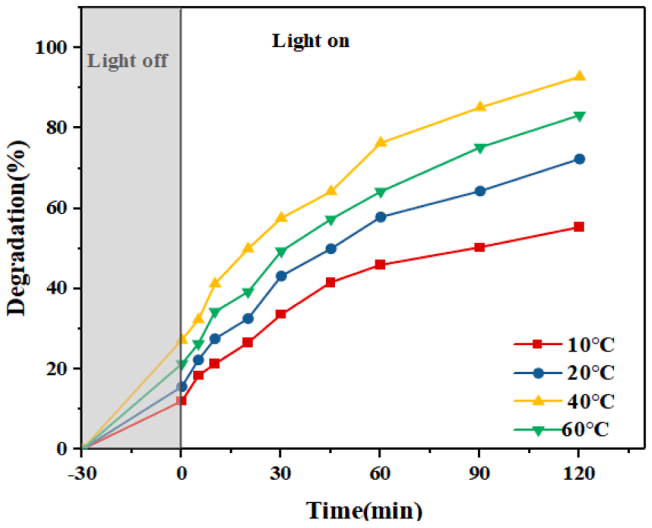

Fig. 11. Effect of temperature on photodegradation of HCQ.

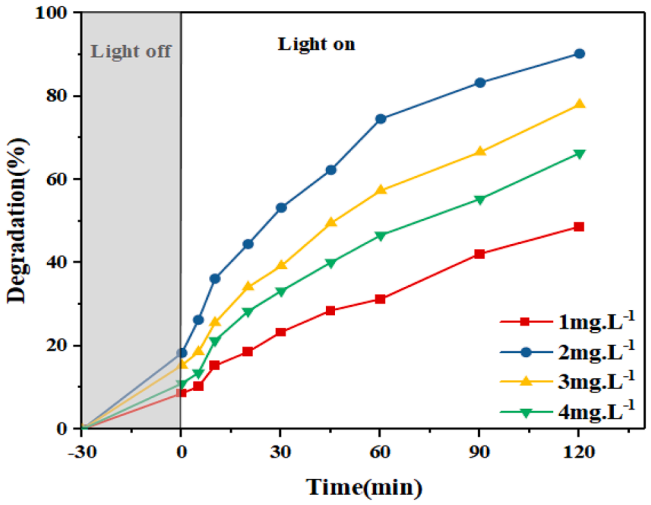

Fig. 12. Effect of different concentrations of H_2O_2 on the photodegradation of HCQ.

increasing the temperature has a natural effect on chemical reactions and increases the degradation process in general by changing the activation energy. An increase in temperature led to an increase in molecules. Kinetic energy had a positive effect because it helps them to move molecules to active regions. As the temperature rises, bubbles formed in the solution, leading to the production of free radicals. In addition, increasing the temperature helps the degradation reaction to overcome a combination of electron holes. Also, increasing the temperature may increase the rate of oxidation of the interface organic molecules [33]. However, with further increases in temperature, the more kinetic energy produced that is able to move the polluting molecules away from the active regions before reaching the degradation process. Therefore, the optimum temperature is 40 °C and after this temperature, the inverse relationship between optical degradation and temperature occurs due to the increase in kinetic energy of the molecules. As a result, the rate of degradation decreased with decreasing hydroxyl production in the solution.

4.1.3. *Effect of hydrogen peroxide (H_2O_2)*

By adding some irreversible electron receptors, including H_2O_2, to the reaction mixture, the recombination of electrons and cavities in photocatalytic reactions can be reduced [34]. Thus, in order to evaluate the ability of photocatalytic degradation with the assistance of H_2O_2, an experiment was performed under catalytic dose of 0.1 g/L, 10 mg/L of the HCQ, and pH 3 with 1–4 mg. L^{-1} H_2O_2under sunlight. The results (Fig. 12) showed that sunlight, catalyst, and H_2O_2 together have a significant effect on the degradation process. Increasing the concentration of oxygen in the solution was very useful for the photocatalytic degradation of the drug. As can be seen, with increasing H_2O_2 concentration, the degradation of pollutant molecules accelerates·H_2O_2 traps electrons and thus prevents the recombination of electron-hole pairs, thereby increasing H_2O_2 probability of OH and O_2 radical formation at the photocatalyst surface. Beyond the optimal concentration of H_2O_2, the rate of hydroxychloroquine degradation reduced due to the radical reduction of OH [1,35]. Subana and Swaminathan reported that increasing the amount of H_2O_2 beyond the optimal level produces more peroxide radicals, which acts as a scavenger for the hole and thus reduces the efficiency of photocatalytic degradation [34]. The accepted mechanism for H_2O_2 is to fracture the O-O bond with the function of sunlight, which causes the formation of a hydroxyl radical (˙OH), which leads to drug degradation [1].

$$H_2O_2 + e^- \rightarrow {}^{\circ}OH + OH^- \quad (1)$$

$$H_2O_2 + {}^{\circ}O_2^- \rightarrow {}^{\circ}OH + OH^- + O_2 \quad (2)$$

$$H_2O_2 + {}^{\circ}OH \rightarrow H_2O + {}^{\circ}OH_2 \quad (3)$$

$${}^{\circ}OH_2 + {}^{\circ}OH \rightarrow H_2O + O_2 \quad (4)$$

$$H_2O_2 \rightarrow H_2O + {}^{\circ}O_2 \quad (5)$$

$$H_2O_2 \rightarrow 2\,{}^{\circ}OH \quad (6)$$

$${}^{\circ}OH + HCQ \rightarrow Degraded\ products \quad (7)$$

The effect of H_2O_2 dose on HCQ degradation can be explained in the number of OH radicals produced and to the absorbance of OH radicals [36]. It is well known that H_2O_2 can trap photoelectron (e^-) to electron-hole pairs (e^- - h^+). Additional OH radicals can be generated by the reaction between H_2O_2 and e^- or $^{\bullet}O_2^-$ (Equations [3] and [4]. Thus, the addition of H_2O_2 to the photocatalytic system leads to the degradation of HCQ. However, beyond the optimal dose, H_2O_2 traps OH radicals to produce weaker oxidizing radicals. Accordingly, trapping of OH radicals occurred through ((Equations. [5] and [6]. The decrease in the concentration of radicals ˙OH produced, due to the higher dose of H_2O_2, inhibited the HCQ degradation. Likewise, the addition of H_2O_2 appears to act as a source of oxygen.

4.1.4. *Effect of different doses of catalyst on photodegradation of HCQ*

The photocatalytic activities of the catalysts under direct sunlight were also evaluated and compared. The optical decomposition curves of HCQ in water as a function of irradiation time in the absence and presence of different doses of catalyst are shown in Fig. 13. Before starting the photocatalytic tests, the solution was kept in the dark for 30 min. Photolysis trials in the absence of catalyst were also performed. As can be seen, the amount of degradation under photolysis and adsorption tests were slight (Fig. 13 a, and b). The solution was then subjected to photocatalytic tests and direct sunlight to evaluate the effect of different doses of catalyst. (Fig. 13c). The photodegradation efficiency achieved at different photocatalyst concentrations of 0.05, 0.1 and 0.2, 0.3 and 0.4 g/L, respectively (38.15), (52.36), (63.57), (91.45) and (80.42). As can be observed, the amount of degradation increased with the increase of the catalyst. Due to the increase in active sites, the rate of photocatalytic degradation of HCQ increases with the photocatalytic dose. The photocatalytic removal mechanism based on the production of OH radicals. Thus, the HCQ contaminant removed through these radicals [37–38]. But beyond the amount (0.3 g/L), due to the increase in

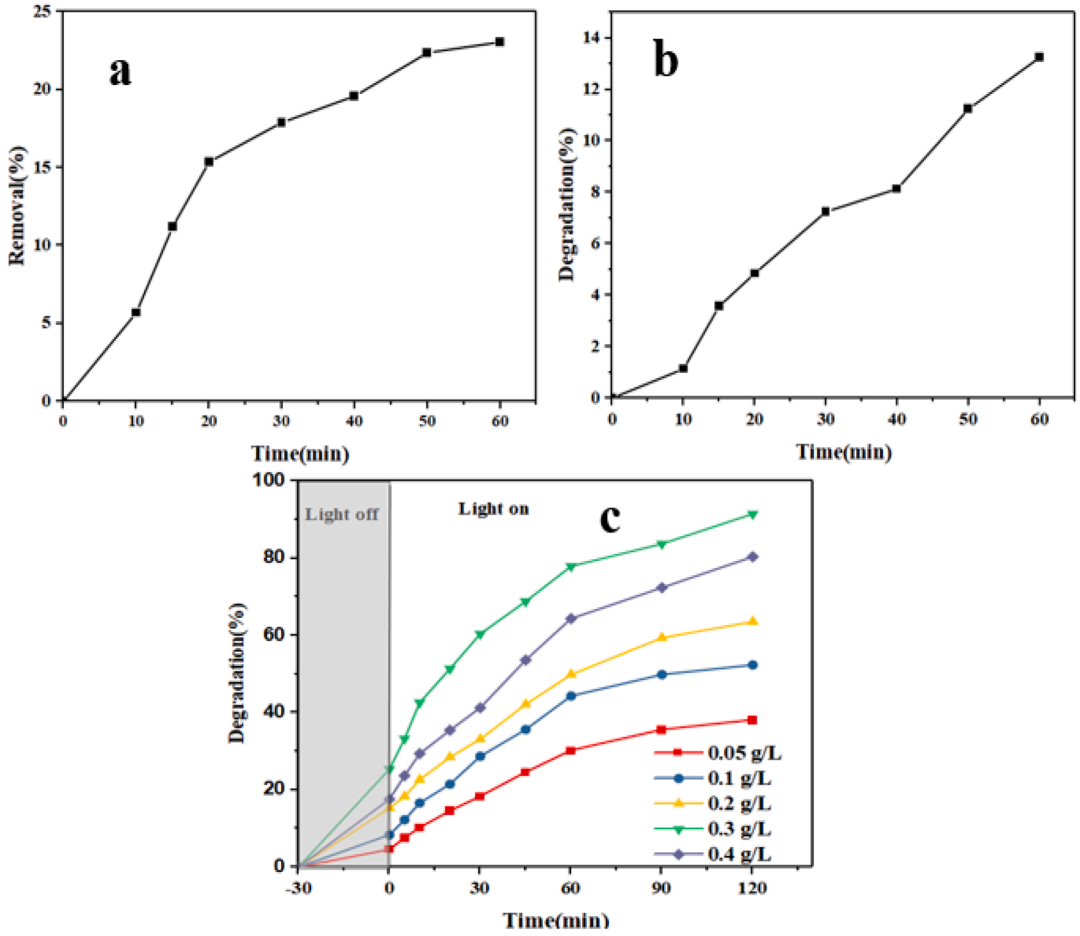

Fig. 13. a: Photolysis, b: Adsorption, and c: Effect of photocatalyst concentration on photocdegradation of HCQ.

turbidity in the solution, the amount of degradation decreased, and thus due to the increase in light scattering and the lower penetration depth of photons, fewer photocatalysts can be activated. In addition, the accumulation of nanoparticles at high concentrations leads to a reduction in the number of surfactant sites available for photocatalytic degradation [39] and inactivation of activated molecules, resulting in the collision of activated molecules with ground-state molecules [40].

4.1.5. Effect of initial concentration HCQ photocatalytic degradation of HCQ

The initial concentration of hydroxychloroquine from 1 to 40 mg/L at pH 3, 0.3 g/L catalyst at a maximum illumination time of 120 min investigated, and the results shown in Fig. 14. As can be seen, increasing the initial concentration of HCQ reduced the degradation efficiency in photolysis and photocatalytic processes. Increasing the HCQ from 1 mg/L to 40 mg/L reduced the removal efficiency of HCQ from (91.89) at a dose of 10 mg/L to (44.26 mg/L) using a catalyst of 0.3 g/L. The reason for this decrease is that increasing the HCQ concentration prevents the efficiency of HCQ removal in the photocatalytic process. This is due to the probability of HCQ contact at a lower concentration is relatively high. However, the relative availability of surface-active sites decreases with increasing HCQ concentration [41]. Higher concentrations of HCQ increased the inhibitory effect and thus reduced the degradation efficiency [38]. Similar results for the photocatalytic degradation of other dye and drug contaminants showed that the surface of catalysts saturated at higher concentrations of contaminants [1].

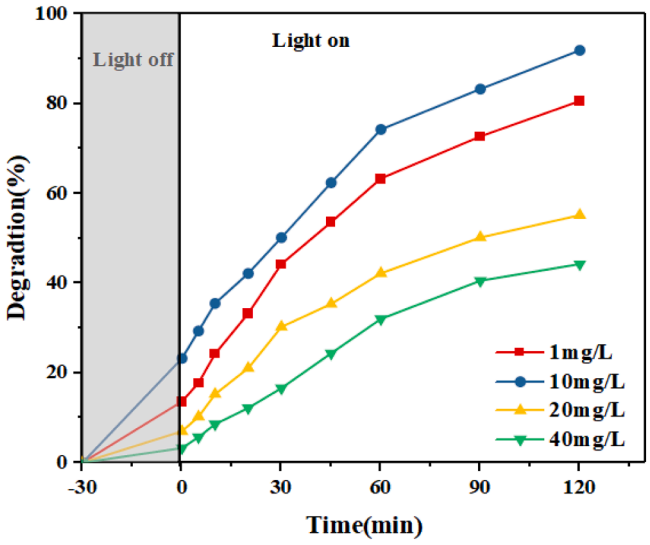

Fig. 14. Effect of initial HCQ concentration on photodegradation of HCQ.

4.2. HCQ degradation kinetics

The time-dependent degradation of HCQ studied under a photocatalytic process. This provides the degradation efficiency and constant stability of the degradation processes. The Kinetics were studied as a function of soluble HCQ concentration. In This study, the optimal

experimental conditions including pH = 3, 10 mg/L concentration of HCQ, catalyst concentration of 0.3 g/L and time of 120 min were considered. C/C_0 values were plotted as a function of time for all concentrations of HCQ under optimal conditions. The results are shown in Fig. 15. The figure clearly shows that an initial sharp decrease in C_t/C_0 in the photocatalytic degradation of HCQ occurred with increasing concentration. The kinetics of the HCQ photodegradation reaction in the presence of the TiO_2/β-Bi_2O_3 catalyst were calculated via Eq.

$$\ln\left(\frac{C}{C_0}\right) = -Kt$$

where C is the instantaneous concentration and C_0 is the initial C, K is the constant reaction rate and t is the reaction time [42]. As Fig. 15 shows, the photodegradation of HCQ is linear over time and followed pseudo-first-order kinetics. Over time, the rate of HCQ degradation reaction decreased from (0.0414) to (0.0129) min^{-1} (Table 1).

4.3. Comparison of photocatalytic degradation of HCQ under UV and sunlight

Due to the difference in photon energy in UV and sunlight, the photocatalytic activity of catalysts may be affected by UV sources. Hence, UV-A was used as a 6-watt UV source for comparison with sunlight in the TiO_2/β-Bi_2O_3 photocatalytic system. The conditions are as follows: 10 mg/L HCQ, 0.3 g/L photocatalyst, pH 3 and 40 °C for 120 min and the results are presented in Fig. 16. The results shown that HCQ degradation occurred with higher efficiency in sunlight compared to UV-A light. So that 90.27% of the degradation was observed in 120 min under UV-A light, while in the presence of sunlight for 120 min with a radiation intensity of 76–72 klux, the degradation was higher with UV-A and 91.89%. In fact, higher intensities of sunlight determine the amount of photons absorbed by the catalyst. By increasing the duration of light irradiation, the catalyst absorbs more photons, which produces more electron-hole pairs on the surface of the catalyst, which increases the concentration of hydroxyl radicals, resulting in higher removal rates. Therefore, it can be inferred that solar photocatalytic degradation can reduce energy costs and stabilize them in areas with high sunlight. In this study, sunlight was more effective than UV light in degrading HCQ contaminants. Solar energy can be substituted as an effective light source due to its abundance, freeness, renewability and non-hazardous nature [35,43].

4.4. A plausible mechanism for reaction

The valence band edge potential (E_{VB}) and the conduction band edge potential (E_{CB}) determine the photocatalytic reaction. E_{VB} was calculated by the following experimental formula.

$$E_{VB} = X - E_e + 0.5E_{bg}$$

$$E_{CB} = E_{VB} - E_{bg}$$

where E_{VB} is the edge potential of E_{VB} E_{bg} is the energy band gap, E_e is the energy of the free electrons on the hydrogen scale (about 4.5 eV), and X is the electronegativity of the semiconductor. E_{bg} is the energy of the semiconductor band gap, which in Fig. 17 corresponds to the DRS spectrum for TiO_2 and β-Bi_2O_3 of 3.2 and 2.46 eV, and the corresponding electronegativity are 5.81 and 6.22 eV. Which was used to calculate the edge of the conduction band (E_{CB}) in the formula [7].As a result, Measured E_{VB} and E_{CB} for TiO_2 were 2.91 and 0.29 eV, respectively, and 2.94 and 0.49 eV for β-Bi_2O_3. Since the conduction band edge for β-Bi_2O_3 nanoparticles was low (0.49 eV), it is not able to provide the sufficiently negative potential for optically excited electrons to reduce the absorbed

Table 1
Parameters affecting HCQ degradation kinetics.

Equation	K(min^{-1})	R^2	HCQ(mg/l)
Y = 0.0414x + 1.7822	0.0414	0.983	1
Y = 0.0334x + 1.4182	0.0334	0.988	10
Y = 0.0221x + 1.1221	0.0221	0.965	20
Y = 0.0129x + 0.3524	0.0129	0.973	40

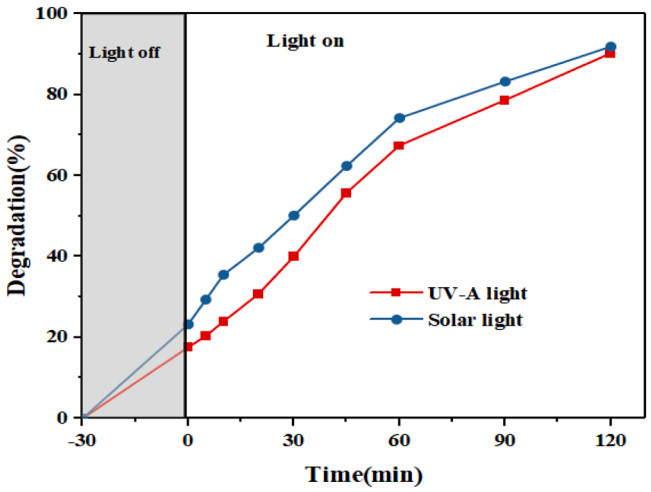

Fig. 16. Comparison of sunlight and UV-A light in HCQ photodegradation.

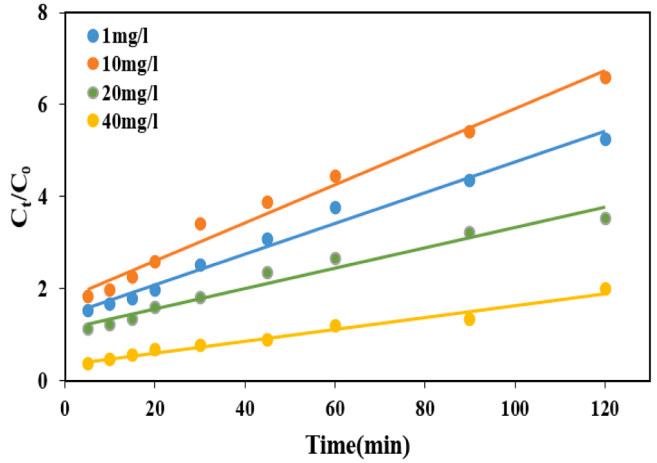

Fig. 15. HCQ degradation kinetics.

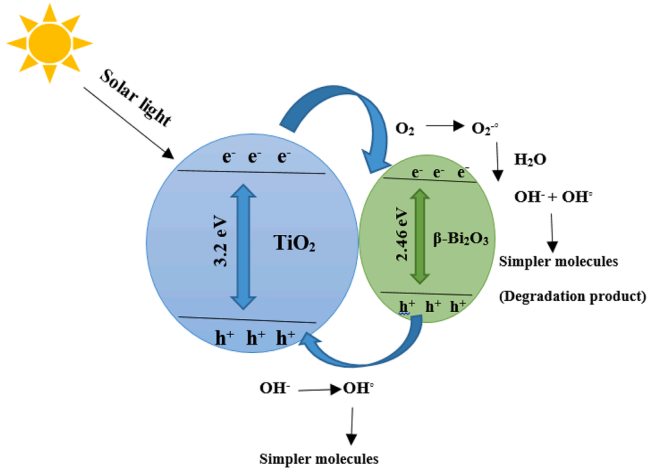

Fig. 17. Proposed mechanism for photocatalytic degradation of HCQ.

O_2 In addition, the E_{CB} for TiO_2 was calculated higher than of the H^+/H_2 decline potential [15]. Therefore, the edge band potential (E_{CB}) of TiO_2 is more active than β-Bi_2O_3. This difference in the conduction band and valence band potentials leads to a potential difference between the two semiconductor catalysts, resulting in the formation of a heterojunction. As a result, the optically generated electron (e^-) migrates from the TiO_2 conduction band to the β-Bi_2O_3 conduction band. Due to the fact that the holes (h^+) move in the opposite direction, the holes on the surface of β-Bi_2O_3 can be transferred to TiO_2 via the potential difference. Therefore, this heterojunction created the interface of the two semiconductors leads to efficient charge separation, thus reducing the recombination of charge carriers (44). Also, on the other hand, the holes produced in VB of TiO_2 can be transferred to VB β-Bi_2O_3 and lead to an increase in the longevity of the generated light charge carriers. In the catalyzed reaction of sunlight, there are many productions of electrons and holes and other oxidative species (ROS). Hence, the photocatalytic efficiency is increased and the HCQ is completely degraded. The schematic reaction pathway on the surface of the TiO_2/β-Bi_2O_3 photocatalyst is shown in Fig. 17.

4.5. Photocatalytic degradation of HCQ at large scale

In this study, the photodegradation of HCQ under a larger-scale photocatalytic system was also investigated Fig 18. For this purpose, a 500 ml container containing HCQ contaminant solution, pH = 3, catalyst concentration of 0.3 g/L, HCQ dose of 10 mg/L was used. The experiment showed that the degradation efficiency of HCQ increased with the passage of time after 120 min, the HCQ degradation efficiency under solar light at large-scale was achieved 70.59%. The results are consistent with the study of Ahmadpour et al. [32] .

4.6. Stability and reusability of the photocatalyst

The reusability of the TiO_2/β-Bi_2O_3 photocatalyst and the removal efficiency of HCQ contaminant was determined as a promising process and a suitable strategy for photocatalytic degradation of the contaminant in each photocatalytic cycle. For this purpose, after each photocatalytic cycle, the TiO_2/β-Bi_2O_3 photocatalyst was separated from the solution and washed several times with distilled water and ethanol, and then dried in an oven at 80 °C for 8 h, and the next step was to remove the HCQ was used [12]. As shown in Fig. 19, it was noticed that upon reusing the nanoparticles for several cycles, the performance of nanoparticles remains the same and there is no remarkable loss in efficiency. The TiO_2/β-Bi_2O_3 catalysts have a relatively stable and reusable activity,

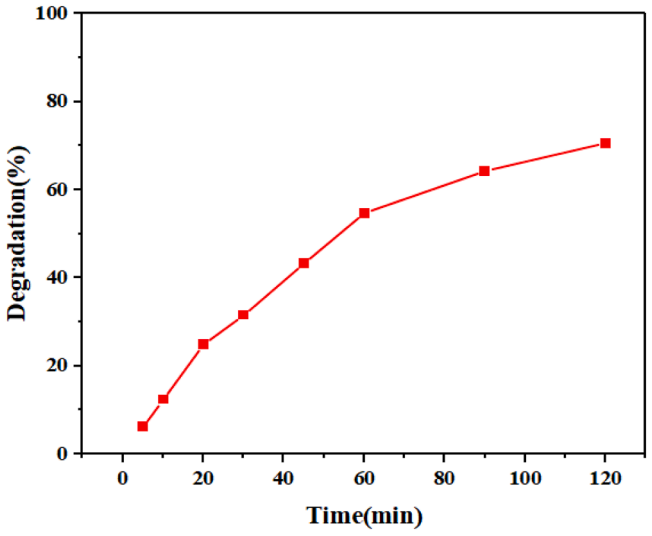

Fig. 18. Impact of large scale on HCQ degradation by TiO_2/ β-Bi_2O_3.

so that after 6 cycles of reuse of the photocatalyst, the photocatalytic degradation of HCQ increased from 91.89% in the first stage to 78.53% decreased in the sixth stage. According to the results, it can be stated that the TiO_2/β-Bi_2O_3 nanoparticles are not disabled during photocatalytic reactions and its application is very economical due to its potential reuse [1].

The superior activity of the prepared photocatalyst originates from the combinatorial factors viz., ordered mesoporous support with high specific surface area and optimum acidity originated from the TiO_2/β-Bi_2O_3; the promotional impact of TiO_2 and combination with β-Bi_2O_3 phase submitted the synergistic advantage. In other words, this high photocatalytic performance can be attributed to the synergistic effect between TiO_2 and β-Bi_2O_3 nanoparticles, narrow bandgap force, and carrier separation [12]. The optimal pH is to be preserved during the photocatalyst synthesis is an important factor to tune the physicochemical characteristics of the photocatalyst and attain high activity.

As mentioned, by changing the pH to acidic the intrinsic and extrinsic attributes of the photocatalyst such as chemical adsorption, surface acidity, surface composition, reducibility, surface morphology, and surface coordination are significantly modified.

XRD and FTIR analysis were performed after 6 reuse cycles to investigate the crystal structure and change the chemical composition of TiO_2/β-Bi_2O_3. The XRD results before and after degradation demonstrated no obvious change in the crystalline structure of TiO_2/β-Bi_2O_3 after six recycles (Fig. 19c). Besides, the FTIR analysis of TiO_2/β-Bi_2O_3 was performed before and after HCQ degradation (Fig. 19b). As Fig. 19b shows, there was not exhibited much change between the four FTIR patterns before and after degradation. According to Fig. 19b, the additional peaks of 3372 cm^{-1} related to O–H tensile vibrations, 1177 cm^{-1} pertained to C-O stretching vibrations, peaks of 1824 and 2767 cm^{-1} pertained to C–H stretching vibrations were observed in the 6th reuse. As noticed, much alteration did not occur in the FTIR peaks before and after the degradation process. This result indicated that TiO_2/β-Bi_2O_3 had excellent chemical stability and can be used as a reusable photocatalyst in most applications.

4.7. Mineralization of HCQ

Photodegradation of HCQ and mineralization with 0.05–0.4 g/l TiO_2/β-Bi_2O_3 catalyst under optimum conditions was evaluated. Fig. 20 indicates the mineralization efficiency within 120 min. As can be seen, the mineralization efficiency (67.84) was acquired in 120 min. The increase in mineralization efficiency in the first hour of light irradiation is due to the absorption of light from the HCQ molecule or the formation of intermediates in the solution. Therefore, it can be seen that the intermediates produced in the solution are not sensitive to photolysis. This means that HCQ has been degraded by the photolysis process, but the sensitivity of intermediaries due to degradation to photolysis was lesser [10,4].

5. Conclusion

In summary, visible light-responsive TiO_2/β-Bi_2O_3 composite nanoparticles were successfully synthesized by the hydrothermal method and used in the degradation of hydroxychloroquine from aqueous solutions. The results showed that these synthesized composite nanoparticles possessed well crystallinity, significant optical properties, and high surface area. This nanocomposite has good nanostructures and dispersion, resulting in a remarkable photocatalytic performance in the photocatalytic degradation of hydroxychloroquine under direct sunlight and UV light. In addition, an acceptable mechanism was proposed for the photocatalytic degradation of hydroxychloroquine by TiO_2/β-Bi_2O_3, and OH and O_2^- radicals were important to the photocatalytic activity. This work not only presents a highly efficient photocatalyst for hydroxychloroquine degradation, but also provides a promising method to remove other contaminants from aqueous solutions for wastewater

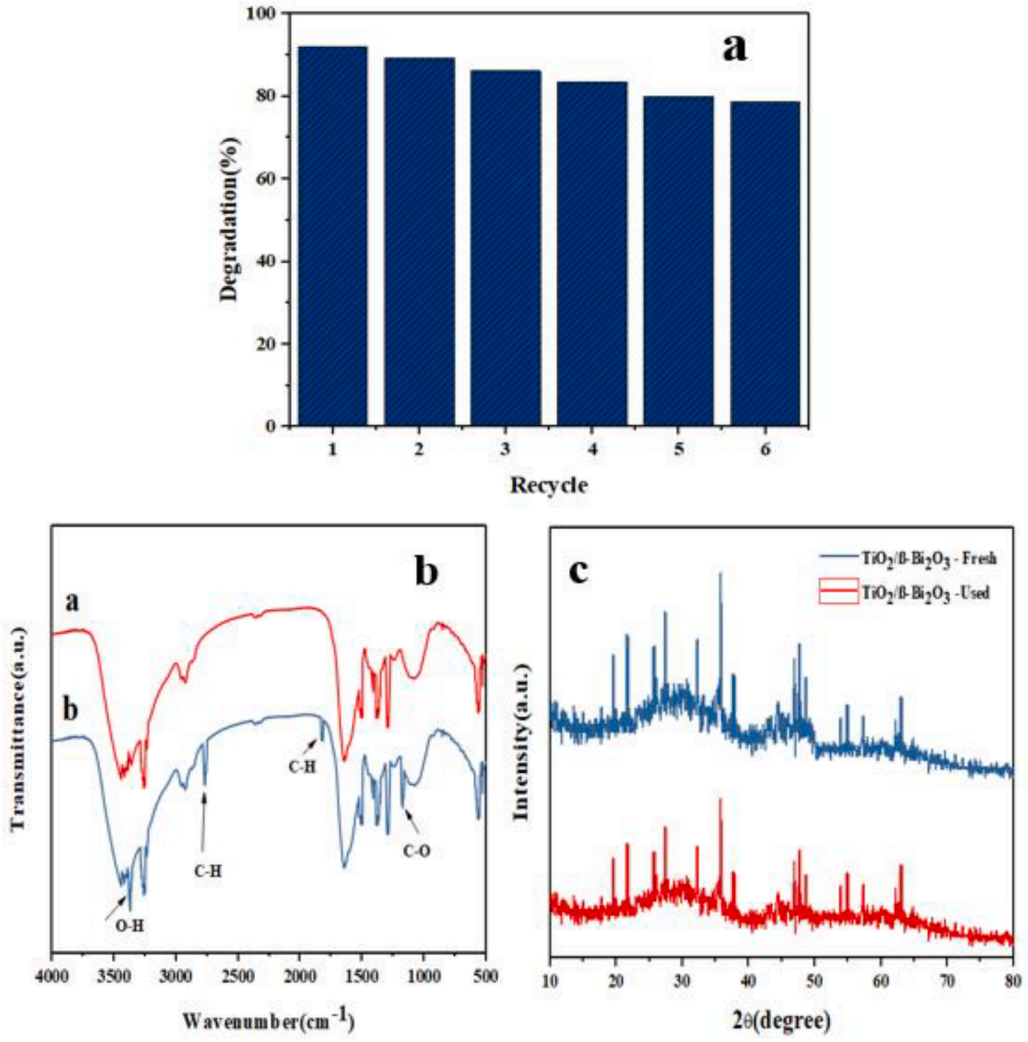

Fig. 19. a) The reusability of TiO_2/β-Bi_2O_3 nanoparticles, b) FTIR spectra of TiO_2/β-Bi_2O_3 a: after and b: before 6 cycles photodegradation, and c) XRD pattern of the photocatalyst before and after 6 cycles photodegradation.

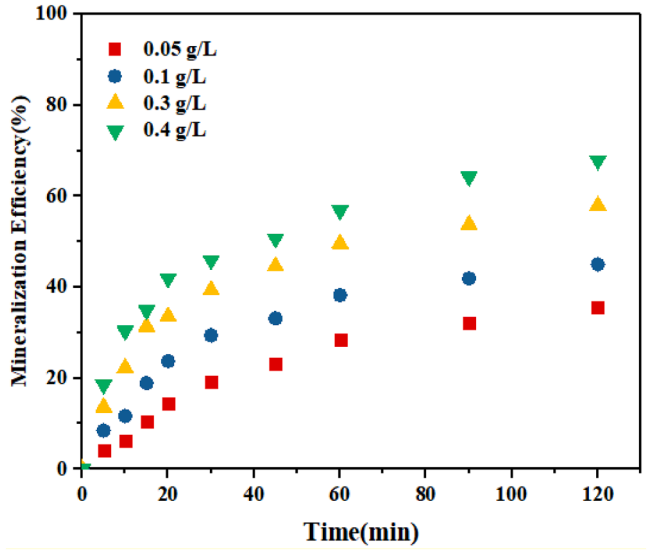

Fig. 20. Mineralization efficiency of HCQ using different TiO_2/β-Bi_2O_3 under optimal conditions.

treatment.

Declaration of Competing Interest

The authors declare that they have no known competing financial interests or personal relationships that could have appeared to influence the work reported in this paper.

Acknowledgement

The paper is from a postgraduate student thesis, Thereby the authors of this research highly appreciate the support of Faculty of Agriculture and Natural Resources, Ardakan University, during the course of the experiments and analysis.

References

[1] M.H. Sayadi, N. Ahmadpour, S. Homaeigohar, Photocatalytic and Antibacterial Properties of Ag-$CuFe_2O_4$@ WO_3 Magnetic Nanocomposite, Nanomater. 11 (2) (2021) 298.
[2] A. Gasmi, M. Peana, S. Noor, R. Lysiuk, A. Menzel, A.G. Benahmed, Chloroquine and hydroxychloroquine in the treatment of COVID-19: the never-ending story, Appl. Microbiol. Biotechnol. 105 (2021) 1333–1343.
[3] S. Dong, L. Cui, Y. Tian, L. Xia, Y. Wu, J. Fan, M. Yu, A novel and high-performance double Z-scheme photocatalyst ZnO-SnO_2-Zn_2SnO_4 for effective removal of the biological toxicity of antibiotics, *HaZ. Mater.* 399 (2020), 123017.

[4] M.H. Sayadi, S. Shekari, H. Sobhani, Photocatalytic degradation of azithromycin using GO@ Fe_3O_4/ZnO/SnO_2 nanocomposites, J. Clean. Prod. 232 (2019) 127–136.

[5] N. Ahmadpour, M.H. Homaeigohar, S. Sayadi, A hierarchical Ca/TiO_2/NH_2-MIL-125 nanocomposite photocatalyst for solar visible light induced photodegradation of organic dye pollutants in water, RSC Adv. 10 (50) (2020) 29808–29820.

[6] M. Stylidi, D.L. Kondarides, X.E. Verykios, Pathways of solar light-induced photocatalytic degradation of azo dyes in aqueous TiO_2 suspensions, Appl. Catal. B: Environm. 40 (4) (2003) 271–286.

[7] G. Žerjav, J. Teržan, P. Djinović, Z. Barbieriková, T. Hajdu, V. Brezová, J. Zavašnik, J. Kovač, A. Pintar, TiO_2-β-Bi_2O_3 junction as a leverage for the visible-light activity of TiO_2 based catalyst used for environmental applications, Catal. Today 361 (2021) 165–175.

[8] J. Rivera-Utrilla, M. Sánchez-Polo, M.Á. Ferro-García, G. Ocampo-Pérez, R. Prados-Joya, Pharmaceuticals as emerging contaminants and their removal from water. A review, Chemosphere 93 (7) (2013) 1268–1287.

[9] H.T. Chang, N.M. Wu, F. Zhu, A kinetic model for photocatalytic degradation of organic contaminants in a thin-film TiO_2 catalyst, Water Res. 34 (2) (2000) 407–416.

[10] N. Ahmadpour, M.H. Sayadi, S. Hajiani, M. Sobhani, A potential natural solar light active photocatalyst using magnetic ZnFe2O4@ TiO2/Cu nanocomposite as a high performance and recyclable platform for degradation of naproxen from aqueous solution, J. Clean. Prod. 268 (2020), 122023.

[11] S. Dong, L. Cui, W. Zhang, L. Xia, S. Zhou, C.K. Russell, M. Fan, J. Feng, J. Sun, Double-shelled $ZnSnO_3$ hollow cubes for efficient photocatalytic degradation of antibiotic wastewater, J. Chem. Eng. 384 (2020) 123279, https://doi.org/10.1016/j.cej.2019.123279.

[12] N. Ahmadpour, M.H. Sayadi, S.H. Sobhani, Photocatalytic degradation of model pharmaceutical pollutant by novel magnetic TiO_2@ $ZnFe_2O_4$/Pd nanocomposite with enhanced photocatalytic activity and stability under solar light irradiation, J. Environ. Manag. 271 (2020), 110964.

[13] S. Dong, Y. Zhao, J. Yang, X. Liu, W. Li, L. Zhang, Y. Zhu, Visible-light responsive PDI/rGO composite film for the photothermal catalytic degradation of antibiotic wastewater and interfacial water evaporation, Appl. Catal. B 291 (2021), 120127.

[14] Y. Xu, Y. Mo, J. Tian, P. Wang, H.Y. Yu, The synergistic effect of graphitic N and pyrrolic N for the enhanced photocatalytic performance of nitrogen-doped graphene/TiO_2 nanocomposites, Appl. Catal. B: Environ. 181 (2016) 810–817.

[15] Huang, Y. Wei, Y. Wang, J. Luo, D. Fan, L. Wu, Controllable fabrication of Bi_2O_3/TiO_2 heterojunction with excellent visible-light responsive photocatalytic performance, Appl. Surf. Sci. 423 (2017) 119–130.

[16] L. Yin, J. Niu, Z.C. Shen, Mechanism of reductive decomposition of pentachlorophenol by Ti-doped β-Bi_2O_3 under visible light irradiation, Environ. Sci. Technol. 44 (14) (2010) 5581–5586.

[17] S. Dong, L. Cui, C. Liu, F. Zhang, K. Li, L.S. Xia, Abrication of 3D ultra-light graphene aerogel/Bi_2WO_6 composite with excellent photocatalytic performance: A promising photocatalysts for water purification, J. Taiwan Inst. Chem. 97 (2019) 288–296.

[18] S. Park, H. Ko, S. Lee, H. Kim, C. Lee, Light-activated gas sensing of Bi_2O_3-core/ZnO-shell nanobelt gas sensors, Thin Solid Films 570 (2014) 298–302.

[19] Y. Lu, Y. Zhao, J. Zhao, Y. Song, Z. Huang, F. Gao, N. Li, Y. Li, Induced aqueous synthesis of metastable β-Bi_2O_3 microcrystals for visible-light photocatalyst study, Cryst. Growth Des. 15 (3) (2015) 1031–1042.

[20] Q. Huang, S. Zhang, C.Z. Cai, B,, β-and α-Bi_2O_3 nanoparticles synthesized via microwave-assisted method and their photocatalytic activity towards the degradation of rhodamine B, Mater. Let. 65 (6) (2011) 988–990.

[21] H.-J. Youn, C. Randall, A. Chen, T. Shrout, M.T. Lanagan, Dielectric relaxation and microwave dielectric properties of Bi 2 O 3-ZnO-Ta 2 O 5 ceramics, J. Mater. Res. 17 (6) (2002) 1502–1506.

[22] S. Iyyapushpam, S.T. Nishanthi, D. Pathinettam Padiyan, Photocatalytic degradation of methyl orange using α-Bi_2O_3 prepared without surfactant, J. Alloys Comp. 563 (2013) 104–107.

[23] N. Ahmadpour, M.H. Sayadi, A. Verma, B. Mansouri, Ultrasonic degradation of ibuprofen from the aqueous solution in the presence of titanium dioxide nanoparticles/hydrogen peroxide, Desalin. Water Treat. 145 (2019) 291–299.

[24] G. Lee, K.H. Chu, Y.A.J. Al-Hamadani, C.M. Park, M. Jang, J. Heo, N. Her, D.-H. Kim, Y. Yoon, Fabrication of graphene-oxide/β-Bi_2O_3/TiO_2/$Bi_2Ti_2O_7$ heterojuncted nanocomposite and its sonocatalytic degradation for selected pharmaceuticals, Chemosphere 212 (2018) 723–733.

[25] J. Tang, T. Zhang, Z. Duan, C. Li, C. Meng, Y. Zhang, Synthesis of Bi_2O_3@ BiOI@UiO-66 composites with enhanced photocatalytic activity under visible light, Chem. Phys. Let. 768 (2021), 138354.

[26] Y. Astuti, A. Fauziyah, S. Nurhayati, A.D. Wulansari, R. Andianingrum, A. R. Hakim, G. Bhaduri, Synthesis of α-Bismuth oxide using solution combustion method and its photocatalytic properties, IOP Conf. Series: Mater. Sci. Eng. IOP Publishing. 107 (2016) 012006.

[27] N. Dhiman, A. Kumar, B.P. Singh, Synthesis and characterization of dye-doped TiO_2-SiO_2 core-shell composite microspheres, J. Nanophotonics 6 (1) (2012), 063511.

[28] S.G.P. Ullattil, P,, A 'one pot'gel combustion strategy towards Ti^{3+} self-doped 'black'anatase TiO_{2-x} solar photocatalyst, J. Mater. Chem. A 4 (16) (2016) 5854–5858.

[29] L.P. Dias, F.C. Correia, J.M. Ribeiro, C.J. Tavares, Photocatalytic Bi_2O_3/TiO_2: N thin films with enhanced surface area and visible light activity, Coatings. 10 (5) (2020) 445.

[30] S. Sood, S.K. Mehta, A. Sinha, S.K. Kansal, Bi_2O_3/TiO_2 heterostructures: synthesis, characterization and their application in solar light mediated photocatalyzed degradation of an antibiotic, ofloxacin, Chem. Eng. J. 290 (2016) 45–52.

[31] N.L. Reddy, S. Emin, M. Valant, M. Shankar, Nanostructured Bi_2O_3@ TiO_2 photocatalyst for enhanced hydrogen production, int. J. Hydrog. Energy. 42 (10) (2017) 6627–6636.

[32] S. Dong, L. Xia, X. Chen, L. Cui, W. Zhu, Z. Lu, M. Fan, Interfacial and electronic band structure optimization for the adsorption and visible-light photocatalytic activity of macroscopic $ZnSnO_3$/graphene aerogel, Compos. B Eng. 215 (2021), 108765.

[33] N. Sobana, K. Selvam, M. Swaminathan, Optimization of photocatalytic degradation conditions of Direct Red 23 using nano-Ag doped TiO_2, Sep. Purif. Technol. 62 (3) (2008) 648–653.

[34] B. Neppolian, H. Choi, S. Sakthivel, B. Arabindoo, V. Murugesan, Solar/UV-induced photocatalytic degradation of three commercial textile dyes, J. Hazard Mater. 89 (2–3) (2002) 303–317.

[35] V. Kruefu, H. Ninsonti, N. Wetchakun, B. Inceesungvorn, P. Pookmanee, S. Phanichphant, Photocatalytic degradation of phenol using Nb-loaded ZnO nanoparticles, Eng. J. 16 (3) (2012) 91–100.

[36] Y. Liu, Y. Ohko, R. Zhang, Y. Yang, Z. Zhang, Degradation of malachite green on Pd/WO_3 photocatalysts under simulated solar light, J. Hazard. Mater. 184 (1–3) (2010) 86–91.

[37] M.H. Sayadi, S. Homaeigohar, A. Rezaei, H. Shekari, Bi/SnO_2/TiO_2-graphene nanocomposite photocatalyst for solar visible light–induced photodegradation of pentachlorophenol, Environ. Sci. Pol. Res. 28 (2020) 15236–15247.

[38] X. Zhang, F. Wu, X. Wu, P.D. Chen, N,, Photodegradation of acetaminophen in TiO_2 suspended solution, J. Hazard. Mater. 157 (2–3) (2008) 300–307.

[39] A. Gnanaprakasam, V. Sivakumar, M. Thirumarimurugan, Influencing parameters in the photocatalytic degradation of organic effluent via nanometal oxide catalyst: a review, Indian J. Mater. Sci. 2015 (2015) 1–16.

[40] F. Poorsajadi, M.H. Sayadi, M. Hajiani, M.R. Rezaei, Synthesis of CuO/Bi_2O_3 nanocomposite for efficient and recycling photodegradation of methylene blue dye, Int. J. Environ. Anal. Chem. 1 (2020) 1–14.

[41] E.S. Elmolla, M. Chaudhuri, Photocatalytic degradation of amoxicillin, ampicillin and cloxacillin antibiotics in aqueous solution using UV/TiO_2 and UV/H_2O_2/TiO_2 photocatalysis, Desalination 252 (1–3) (2010) 46–52.

[42] M. Muruganandham, M. Swaminathan, Photochemical oxidation of reactive azo dye with UV–H_2O_2 process, Dyes. Pigms. 62 (3) (2004) 269–275.

[43] N. Wei, H. Cui, C. Wang, G. Zhang, Q. Song, W. Sun, X. Song, M. Sun, J. Tian, Bi_2O_3 nanoparticles incorporated porous TiO_2 films as an effective p-n junction with enhanced photocatalytic activity, J. Am. Ceram. Soc. 100 (4) (2017) 1339–1349.